Ground-state wave functions of Tb^{3+} ions in paramagnetic $TbPO_4$: A neutron scattering study

C.-K. Loong, L. Soderholm, and G. L. Goodman
Intense Pulsed Neutron Source, Chemistry and Materials Science Division, Argonne National Laboratory, Argonne, Illinois 60439-4814

M. M. Abraham and L. A. Boatner
Solid State Division, Oak Ridge National Laboratory, Oak Ridge, Tennessee 37831-6056
(Received 23 April 1993)

The paramagnetic-excitation spectrum of $TbPO_4$ has been investigated by means of inelastic neutron-scattering techniques, and the observed crystal-field transitions were analyzed using a Hamiltonian that included the atomic free-ion and crystal-field interactions for an f^8 configuration. Five parameters for the crystal-field potential were obtained that provided a satisfactory description of the neutron data collected at temperatures between 4.2 and 150 K. The calculated crystal-field contribution to the specific heat in the 4–10 K temperature range and the paramagnetic susceptibility agree well with the experimental results. The large anisotropy of the magnetic ground-state doublet of the Tb ions with respect to the crystallographic c axis has important consequences for the spin structure in the antiferromagnetic phases at low temperatures. The effective internal magnetic field in antiferromagnetic $TbPO_4$ was estimated based on the crystal-field-level scheme and a molecular-field approximation and was found to be in good agreement with the values reported from other measurements.

I. INTRODUCTION

A number of investigations,[1–21] both experimental and theoretical, have previously been undertaken in attempts to understand the intriguing physical properties of $TbPO_4$. At low temperatures, this compound exhibits two magnetic phase transitions: an antiferromagnetic ordering of the Tb moments along the crystallographic c axis of the tetragonal zircon structure at 2.28 K and a tilting of the magnetic moments away from the c axis in the (110) planes below 2.15 K.[1–3] The latter transition is accompanied by a cooperative Jahn-Teller effect involving Tb ion-lattice coupling that induces a tetragonal-to-monoclinic distortion of the crystal lattice and a readjustment of the Tb electronic states as required by the lowering of the rare-earth site symmetry. An anomalous behavior of the Young's modulus and lattice parameters of $TbPO_4$ (in comparison with nonmagnetic YPO_4) was found in the temperature range of 10–150 K.[4] The crystal-field states and the spin dynamics of the Tb^{3+} ions have important consequences for the magnetic and luminescence properties of $TbPO_4$, which are manifested in the magnetic susceptibility,[11–14] magnetization,[6,13,14] specific heat,[9–13] magnetic phase transitions,[20,21] and in the optical-adsorption/emission spectra.[5–8] A characterization of the electronic wave functions of the crystal-field states and the nature of the spin-spin and spin-lattice interactions is useful for understanding both the bulk and microscopic properties of the material.

In spite of numerous prior studies employing various experimental methods, information regarding the crystal-field-split ground-multiplet wave functions of Tb^{3+} ions in $TbPO_4$ is still incomplete. Table I lists some of the previous significant experimental findings. The susceptibility and specific-heat measurements indicated do not provide sufficient sensitivity for an accurate assessment of the energies and symmetry of the crystal-field states, and spectroscopy remains the method of choice for this purpose. From optical-absorption and Zeeman-effect measurements, Böhm and co-workers[5] deduced a crystal-field-level scheme for the ground $^7F_6$ and the higher-energy $^5D_4$ multiplets of the Tb ions in $TbPO_4$. The crystal-field parameters derived solely from the observed data for the $^7F_6$ multiplet, however, differ from those obtained from a similar study by Lewis and Prinz.[7] These results are also different from those obtained from fitting the susceptibility[16] and magnetization[14] data (see Table I).

Magnetic neutron scattering probes the low-lying electronic states via magnetic dipole transitions as opposed to the electric dipole transitions between the ground state and the significantly higher-energy states normally observed in an optical study. Therefore, these two techniques provide complementary information regarding the energy-level structure of the magnetic ions. Moreover, unlike optical spectroscopy, neutron-scattering cross sections for crystal-field transitions can be calculated sufficiently reliably to permit a quantitative comparison to be made with the observed intensities. In fact, in a recent systematic study[22,23] of the rare-earth orthophosphates, we have found that the crystal-field parameters obtained from a combined treatment of the neutron and optical data can facilitate a more consistent description of the magnetic properties. In this paper, we present the results of a neutron-scattering study of crystal-field excitations in $TbPO_4$ at selected temperatures from 4.2 to 150 K along with a corresponding determination of the crystal-field parameters using a crystal-field model formulated by spherical tensor techniques based on the scheme of intermediate coupling. The calculated excitation spec-

tra agree well with both the neutron and optical data. The calculated paramagnetic susceptibility and specific heat are also compared with the data previously reported in the literature. Finally, the energy scale for the spin-spin interactions, in terms of an exchange field strength and at temperatures precursory to the magnetic phase transitions, is estimated from the observed intrinsic linewidths of the crystal-field transitions at 4.2 K.

II. EXPERIMENTAL DETAILS

About 80 g of polycrystalline samples of $TbPO_4$ and $LuPO_4$ were prepared by coprecipitation of the rare-earth oxide and ammonium hydrogen phosphate in molten urea followed by a calcination at 800 °C to remove the urea.[24] The samples, in the form of a fine powder, were examined by x-ray diffraction and were found to exhibit

TABLE I. Properties of $TbPO_4$.

	Temperature range	Parameters	Experiment	Ref.
Crystal structure	2.15–300 K	Tetragonal, space group $I4_1/amd$ Tb site symmetry $\bar{4}2m$	X-ray diffraction Neutron diffraction	1–3
	<2.15 K	Monoclinic, space group $C2$ Tb site symmetry 2		
Thermal expansion relative to YPO_4	10–150 K	$\delta\left[\frac{\Delta a}{a}\right]=5.5\times10^{-4}$, $\delta\left[\frac{\Delta c}{c}\right]=-4.0\times10^{-4}$, where $\delta\left[\frac{\Delta l}{l}\right]=\left[\frac{\Delta l(10K)}{l(290K)}-\frac{\Delta l(150K)}{l(290K)}\right]_{TbPO_4}-\left[\frac{\Delta l(10K)}{l(290K)}-\frac{\Delta l(150K)}{l(290K)}\right]_{YPO_4}$	X-ray diffraction	4
Relative Young's modulus	2 K	$E(2K)/E(100K)-1=-0.33$		4
Magnetic structure	2.15–2.28 K	Antiferromagnetic, spins colinear $\|c$ axis	Neutron diffraction	1,2
	<2.15 K	Antiferromagnetic, spins tilted off the c axis in the (110) planes		
Saturated moment	0 K	$7.9\mu_B$ $6.36\mu_B$	Neutron diffraction Neutron spectroscopy	1 a
Néel temperature		$T_{N1}=2.28\pm0.02$ K $T_{N2}=2.15\pm0.02$ K	Neutron diffraction Optical spectroscopy Specific heat Magnetic susceptibility Magnetoelectric susceptibility	1,2 5–8 9–13 11–14 15,19
Effective internal field strength	<2.15 K	4.5±0.15 kG 5.5 kG, 7.2±0.2 kG 5.23 kG	Zeeman splittings Magnetization Neutron spectroscopy	5 5,6,13 a
g factors for ground-state doublet		$g_\parallel=12.25$, $g_\perp=0$ $g_\parallel=12.73$, $g_\perp=0$	Magnetic susceptibility Neutron spectroscopy	16 a
Crystal-field parameters (cm^{-1})		B_0^2 B_0^4 B_0^6 B_4^4 B_4^6		
		352 112 −800 −848 151	Optical spectroscopy	5
		426 200 −688 −999 −641	Far-infrared spectroscopy	7
		410 200 −688 999 413	Magnetization	14
		357.6 125 −848 −866 160	Magnetic susceptibility	16
		356.5 118.9 −790.4 −798.5 −119.1	Neutron spectroscopy	a

[a]Present work.

the appropriate tetragonal zircon structure.[25] No impurity phases were observed within the experimental uncertainty. The powder samples were then pressed into pellets and annealed at 1200 °C in air for 24 h, since such heat treatments are known to promote grain growth and improve the crystalline quality.[24]

The neutron-scattering experiments were carried out using the high-resolution medium-energy chopper spectrometer (HRMECS) at the intense pulsed neutron source of Argonne National Laboratory. The energy resolution ΔE (full width at half maximum) of the HRMECS spectrometer varies between 2–4% of the incident-neutron energy (E_0) over the neutron-energy-loss region, $E=E_0-E_1>0$ (where E_1 is the scattered-neutron energy).[26] For example, $\Delta E \approx 2$ meV at $E=20$ meV for $E_0=60$ meV, whereas $\Delta E \approx 0.12$ meV at $E=2$ meV for $E_0=4$ meV. Measurements of the isostructural, nonmagnetic reference compound $LuPO_4$ under identical experimental conditions were made in order to estimate the contributions from nuclear elastic and phonon scattering. The data were corrected for background scattering by subtracting the results for empty-container runs. Measurements of the elastic incoherent scattering from a vanadium standard provided detector calibration and intensity normalization. The samples were cooled by either a closed-cycle helium refrigerator or a conventional cryostat with the sample temperature controlled at a selected temperature within 0.1 K throughout a run.

III. RESULTS AND DISCUSSION

Rare-earth orthophosphates, RPO_4, form in either the monoclinic crystal structure (monazite for $R=$La to Gd, space group $P2_1/n$) or the tetragonal zircon structure (xenotime for $R=$Tb to Lu, space group $I4_1/amd$).[27] Although the monoclinic phase of $TbPO_4$ can also be stabilized,[28] the $TbPO_4$ sample synthesized for this study had the zircon structure, and no evidence for the presence of a monoclinic phase was found from x-ray diffraction. In the zircon structure, the rare-earth ions are located at sites of D_{2d} point-group symmetry. Consequently, the ground $^7F_6$ multiplet of the Tb^{3+} ions is split by the crystal field into seven singlets, $2\Gamma_1+\Gamma_2+2\Gamma_3+2\Gamma_4$, and three doublets, $3\Gamma_5$. The magnetic-dipole transitions allowed in a neutron-scattering experiment are $\Gamma_1\leftrightarrow\Gamma_2$, $\Gamma_1\leftrightarrow\Gamma_5$, $\Gamma_2\leftrightarrow\Gamma_5$, $\Gamma_3\leftrightarrow\Gamma_4$, $\Gamma_3\leftrightarrow\Gamma_5$, $\Gamma_4\leftrightarrow\Gamma_5$, and $\Gamma_5\leftrightarrow\Gamma_5$. The next higher multiplet $^7F_5$ is located at about 2100 cm^{-1}, and transitions to the states of this and other multiplets cannot be observed in the present neutron-scattering study. (1 meV is equivalent to 8.066 cm^{-1}, and these two units of energy will be used interchangeably here.) In optical spectroscopy using visible light, electric dipole transitions between the ground state and states in the high-energy multiplets give rise to strong absorption and/or emission-line intensities, and all of the nine states in the $^5D_4$ multiplet at about 20 500 cm^{-1} were resolved previously by Böhm and co-workers[5] by optical spectroscopy. Additional information regarding the low-lying crystal-field states has been obtained from far-infrared absorption of the Zeeman-splitting energies, and two different schemes for the Tb^{3+}, $^7F_6$ ground multiplet have been proposed by Böhm and co-workers[5] and by Lewis and Prinz[7] based on far-infrared studies.

In a neutron magnetic-scattering experiment crystal-field transitions give rise to sharp peaks in the observed spectrum. The observed position of a crystal-field peak is equal to the energy separation of the two crystal-field states (e.g., $|m\rangle$ and $|n\rangle$) that participate in the transition, and the intensity is proportional to the square of the matrix element $\langle n|J_\perp|m\rangle$ (where $J_\perp$ is the component of the total angular-momentum operator perpendicular to the neutron wave vector).[29] The intrinsic width of a crystal-field peak provides, in principle, a measure of the energy scale of interactions between a magnetic ion and its environment. If the crystal-field-state energies and wave functions are obtained from a diagonalization of a Hamiltonian that contains a parameter set for the crystal-field potential, then the neutron-scattering function $S(E)$ can be calculated in a straightforward manner. Details concerning the neutron-scattering cross section, the differentiation between magnetic- and nuclear-scattering processes, the relation between the observed transition strengths, and the spectroscopic splitting g factors have been given elsewhere.[22,23] In practice, the crystal-field parameters for the system under study are not known, and the goal is to find a set of crystal-field parameters that produces calculated spectra which are consistent with the observed crystal-field peak energies and intensities at all temperatures.

$TbPO_4$ is expected to exhibit a complex crystal-field excitation spectrum, since there are many allowed transitions. Some of these, however, may be too weak to observe or too close in energy to resolve experimentally. Therefore, it is important to collect data over a wide range of temperatures so that changes in the overall spectrum, as higher-lying states become populated with increasing temperatures, can be analyzed collectively. The spectra observed at selected temperatures from 4.2 to 150 K are shown in the upper panels of Figs. 1 to 3. For neutron incident energies E_0 of 4 meV (Fig. 1), 20 meV (Fig. 2), and 60 meV (Fig. 3) the instrumental resolutions (about 3% of E_0) were optimized for measurements of energy transfers in the 0–3, 5–15, and 15–40 meV ranges, respectively. The phonon background is small ($<10\%$), particularly at low temperatures, therefore, the observed intensities can be accounted for by considering only magnetic scattering. The magnetic, elastic component at zero-energy transfer can be identified from the 4-meV run (labeled A in Fig. 1) because for the detector angles of 3–20° at such low incident energy, nuclear-coherent Bragg scattering is absent. Thus, the presence of strong elastic scattering implies that the Tb^{3+} ground state is a magnetic Γ_5 doublet—as also indicated by the optical measurements.[5,7] Major inelastic peaks were observed at about 0.46, 0.97, 2.6, 6.8, 9.2, and 20.2 meV. A very weak magnetic feature at about 31.2 meV (labeled P in Fig. 3) was also identified after a careful examination of the temperature and wave-vector dependence and a comparison with the $LuPO_4$ spectra. [The broad peak at about 35 meV, which appears in all the RPO_4 ($R=$Tb to

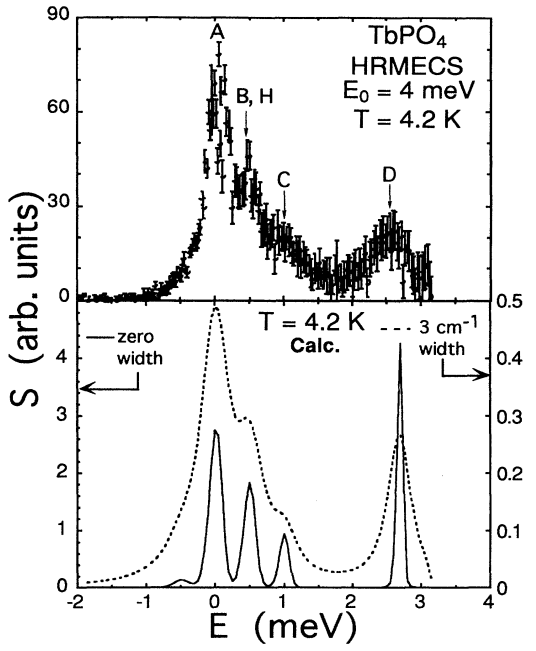

FIG. 1. Upper panel: The measured scattering functions for $TbPO_4$ at 4.2 K with a neutron incident energy of 4 meV. The labeled peaks correspond to the crystal-field transitions shown in Fig. 4. Lower panel: The calculated scattering functions for crystal-field transitions for $TbPO_4$ at 4.2 K. The assumed widths of the Lorentzian functions for crystal-field transitions are 0 (solid curve) and 3 cm^{-1} (dashed curve). The calculated spectra have been convoluted with the instrumental resolution function (ΔE varies smoothly from about 2 cm^{-1} on the left to 0.7 cm^{-1} on the right of the spectrum).

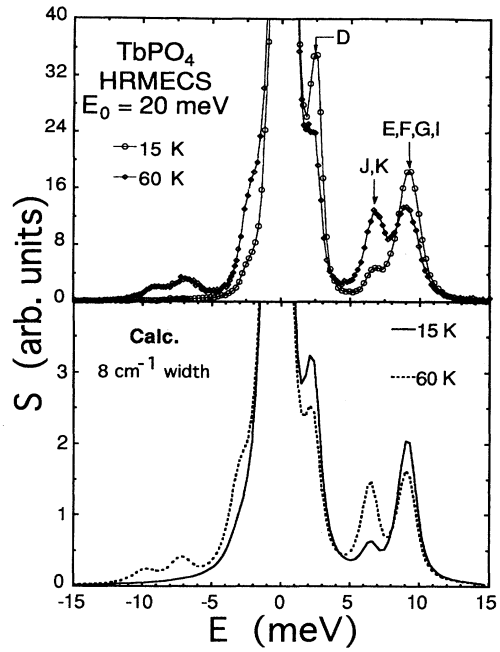

FIG. 2. Upper panel: The measured total-scattering functions for $TbPO_4$ at 15 and 60 K with a neutron incident energy of 20 meV. The data point errors are approximately the size of the symbols. The lines are guides to the eye. The labeled peaks correspond to the crystal-field transitions shown in Fig. 4. Lower panel: The calculated scattering functions for crystal-field transitions of $TbPO_4$ at 15 and 60 K. The assumed widths of the Lorentzian functions for crystal-field transitions at both temperatures are 8 cm^{-1}. The calculated spectra have been convoluted with the instrumental resolution function (ΔE varies smoothly from about 8 cm^{-1} on the left to 3 cm^{-1} on the right of the spectrum).

Lu) spectra, originates from phonon scattering.] The intensities of all these magnetic peaks decrease with increasing temperature except for the peak at 6.8 meV, which increases with increasing temperature. This indicates that the peaks at 0.46, 0.97, 2.6, 9.2, and 20.2 meV originate from crystal-field excitations of the ground states, and the 6.8-meV peak arises from transitions from low-lying excited states. Deexcitations from thermally occupied states to the ground states are also observed as neutron energy-gain processes ($E<0$) in Figs. 1–3, but they are not well resolved because of the relatively poor resolution in this region. The energy resolutions ΔE in the optimized energy-transfer regions of Figs. 1–3, on the other hand, are significantly smaller than the observed linewidths of the peaks. This indicates that the peaks are broadened intrinsically by interactions of the Tb moments with the environment and/or they are comprised of multiple transitions of nearly the same energies. In order to understand the energy-level structure of the Tb ions, both the positions and the temperature dependence of the observed intensities have to be analyzed quantitatively by utilizing a crystal-field model.

The crystal-field model employed here represents a single rare-earth ion in a crystalline environment. The formulation is based on the scheme of intermediate coupling using spherical-tensor techniques. The full Hamiltonian [which includes atomic free-ion and crystal-field interactions for an f^N configuration ($N=8$ for a Tb^{3+} ion)], the associated parameters, and underlying assumptions of the theory have been treated in detail elsewhere[30,31]—hence, only the procedure for the refinement of the crystal-field parameters is outlined here. The crystal-field portion of the Hamiltonian can be written as

$$H_{\mathrm{CF}}=\sum_{k,q,i} B_q^k[C_q^k(i)+C^k_{-q}(i)], \quad k\geq q\geq 0\ , \tag{1}$$

where the $C_q^k(i)$ are spherical tensor operators of rank k and depend on the coordinates of the ith electron. The summation of i is over all f electrons of the ion, and the B_q^k are the crystal-field parameters. For Tb ions occupying lattice sites of tetragonal (D_{2d}) symmetry, the crystal-field potential is characterized by five parameters of real numbers: B_0^2, B_0^4, B_4^4, B_0^6, and B_4^6. A simultaneous change of the signs of B_4^4 and B_4^6, corresponding to a 45° rotation about the unique axis, would affect the polarizations but not the energy-level results. The full Hamiltonian is diagonalized using up to 300 states of the f^8

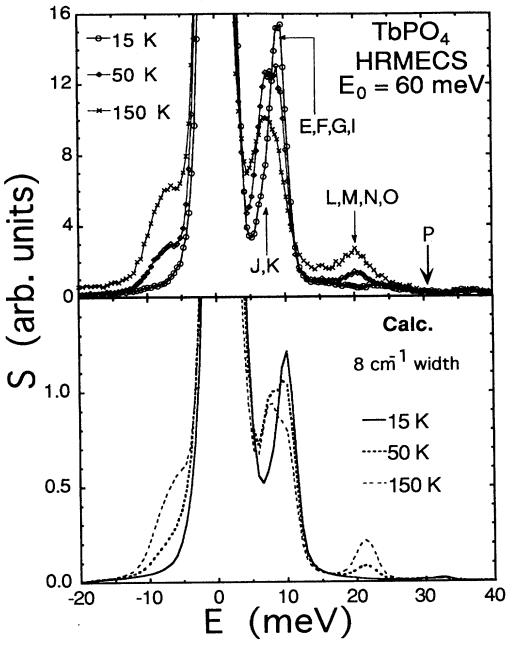

FIG. 3. Upper panel: The measured total-scattering functions for $TbPO_4$ at 15, 50, and 150 K with a neutron incident energy of 60 meV. The data point errors are approximately the size of the symbols. The lines are guides to the eye. The labeled peaks correspond to the crystal-field transitions shown in Fig. 4. Lower panel: The calculated scattering functions for crystal-field transitions of $TbPO_4$ at 15, 50, and 150 K. The assumed widths of the Lorentzian functions for crystal-field transitions at all temperatures are 8 cm^{-1}. The calculated spectra have been convoluted with the instrumental resolution function (ΔE varies smoothly from about 24 cm^{-1} on the left to 10 cm^{-1} on the right of the spectrum).

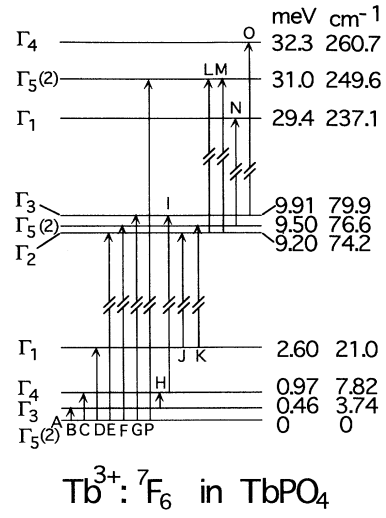

FIG. 4. A schematic diagram of the splitting of the Tb^{3+} $^7F_6$ ground multiplet by the crystal field into seven singlets, $2\Gamma_1+\Gamma_2+2\Gamma_3+2\Gamma_4$ and three doublets, $3\Gamma_5$. The transition labels refer to the experimentally observed transitions shown in Figs. 1–3.

configurations for a Tb^{3+} ion utilizing a computer code developed by Crosswhite and Crosswhite.[31] Since the low-lying crystal-field states are insensitive to the free-ion part of the Hamiltonian, we have adopted the Tb^{3+} free-ion parameters that were established for Tb^{3+} in a LaF_3 host,[32] and the free-ion parameters were fixed in the refinement of the crystal-field parameters.

Guided by the selection rules and the assigned states given in an optical study of $TbPO_4$ by Böhm and co-workers,[5] the fitting of the observed neutron spectra with the crystal-field model was straightforward, yielding calculated energies and transition strengths in good agreement with experimental results for all of the transitions at different temperatures. The resulting crystal-field level scheme for the Tb^{3+} $^7F_6$ ground multiplet is shown schematically in Fig. 4, and the calculated magnetic neutron-scattering spectra are displayed in the lower panels of Figs. 1–3. Details concerning the magnetic form factor and the instrumental resolution functions in use have been described previously, and the procedures were thoroughly tested for the cases of $TmPO_4$, $HoPO_4$, and $ErPO_4$.[22,23] As can be seen in Fig. 4, the 13 states within the $^7F_6$ ground multiplet are split into three groups of closely spaced levels in the regions of 0–2.6, 9–10, and 29–33 meV. Since each group contains a Γ_5 doublet which may connect to all other states with nonzero-transition matrix elements, the resulting spectrum consists of transition energies too close to be resolved experimentally. In the present case, fitting all the data with the model used to calculate both the *energies* and the *matrix elements* $\langle n|J_\perp|m\rangle$ involving all the states is essential to the determination of the five crystal-field parameters. This method imposes stringent conditions on the goodness of fit. The calculated scattering function S as shown in Figs. 1–3, agree well with the observed spectra. The excitations at 6.8 meV actually contain contributions from two transitions J and K (see also Fig. 4). Similarly, the peaks at 9.2 and 20.2 meV each are composed of four transitions: E, F, G, I and L, M, N, O, respectively. In addition, diagonalization of the full Hamiltonian allows the fitting of both the low-lying states derived from neutron data as well as the high-energy states resolved by optical spectroscopy. Since only seven energies belonging to the crystal-field split $^5D_4$ multiplet were observed by Böhm and co-workers,[5] we have refined only one electrostatic parameter F^2 (F^2 changed from 88 995 to 92 683 cm^{-1}) and reached a reasonable agreement characterized by a root-mean-square energy deviation of 7.5 cm^{-1} for the $^5D_4$ multiplet near 20 500 cm^{-1} (2.54 eV). The crystal-field parameters and the wave functions of the $^7F_6$ ground-multiplet states are given in Tables I and II, respectively.

The present analysis also permits an estimate to be made of the intrinsic widths of the transitions. The intrinsic width of an observed crystal-field peak represents a measure of the lifetime of the transition. At elevated temperatures the probability of decay through coupling with other mediating excitations such as phonons in-

TABLE II. The ground-state multiplet wave functions of Tb^{3+} ions in $TbPO_4$.

$^7F_6$ states	E^{obs} (cm^{-1})	E^{calc} (cm^{-1})	Wave functions
Γ_5	0.0	0.0	$\mp 0.33\|\pm 1\rangle \mp 0.19\|\mp 3\rangle \mp 0.92\|\mp 5\rangle$
Γ_3	3.71±0.8	3.74	$0.20(\|2\rangle+\|-2\rangle)+0.68(\|6\rangle+\|-6\rangle)$
Γ_4	7.82±1	7.85	$0.70(\|6\rangle-\|-6\rangle)$
Γ_1	21.0 ±0.8	21.0	$0.60(\|4\rangle+\|-4\rangle)+0.53\|0\rangle$
Γ_2	74.2±1	74.2	$-0.70(\|4\rangle-\|-4\rangle)$
Γ_5		76.6	$\pm 0.51\|\pm 1\rangle -0.14\|\pm 3\rangle \pm 0.77\|\mp 3\rangle \mp 0.34\|\pm 5\rangle$
Γ_3		79.9	$0.68(\|2\rangle+\|-2\rangle)-0.20(\|6\rangle+\|-6\rangle)$
Γ_1	237.1±4	237.1	$-0.37(\|4\rangle+\|-4\rangle)+0.85\|0\rangle$
Γ_5	251.6±7	249.6	$\mp 0.39\|\pm 1\rangle +0.69\|\mp 1\rangle -0.52\|\pm 3\rangle$
			$\pm 0.29\|\mp 3\rangle -0.14\|\mp 5\rangle$
Γ_4		260.7	$0.70(\|2\rangle-\|-2\rangle)$

creases. We find that the broadening of the crystal-field lines at $T \geq 15$ K can be accounted for by assuming an intrinsic width of approximately 8 cm^{-1} (at $T=4$ K, the intrinsic width is ~ 3 cm^{-1}, see Figs. 1–3). At 4.2 K the observed transitions A–D are significantly broader than the instrumental resolution shown by the solid curve in the lower panel of Fig. 1. These results are consistent with the unusually broad lines observed in the high-resolution optical-absorption spectra down to 2.3 K.[5] Since phonon contribution to the line broadening below 4 K is expected to be negligible, these residual linewidths are probably due to superexchange interactions of the Tb magnetic moments via the oxygen ligands.

The crystal-field states derived from neutron scattering can be used to calculate the magnetic contributions of the Tb ions to the paramagnetic susceptibility and specific heat of $TbPO_4$. In Fig. 5, the calculated van Vleck susceptibility[22,33] is compared with the bulk susceptibility of $TbPO_4$ obtained from single-crystal measurements by Sen, Heogy, and Wanklyn[16] and by Androneko *et al.*[14] In general, the agreement between the calculated and observed susceptibility is good over the temperature range of 10–300 K. Below 50 K, however, some systematic difference in $\chi_\parallel$ between the calculation and experiment is noted (see the inset of Fig. 5). Similar disagreement exists also in the analyses of the susceptibility data by Sen, Heogy, and Wanklyn[16] and Andronenko *et al.*[14] This discrepancy is probably caused by exchange interactions of the magnetic moments at low temperatures which are not taken into account in the single-ion crystal-field calculations. The large anisotropy in $\chi_\parallel$ versus $\chi_\perp$ arises from the large (92%) components of $|6,\pm 5\rangle$ in the ground-state Γ_5 doublet wave functions (see Table II). The spectroscopic splitting factors $g_\parallel$ and $g_\perp$ of the Γ_5 doublet are calculated to be 12.73 and 0, respectively, in good agreement with those obtained from magnetization and susceptibility measurements (12.0±0.3 and 0 by Schopper;[12] 12.25 and 0 by Sen, Heogy, and Wanklyn[16]). The "easy" axis, being the crystallographic c axis, coincides with the directions of the ordered moments when the system enters the first antiferromagnetic phase as the temperature drops below 2.28 K. Böhm and co-workers[5] have adopted the semiclassical model of Pytte and Stevens[34] in order to argue that the crystal-field potential of the Tb ions in $TbPO_4$ also favors a tilt of the moments in the (110) planes—as manifested by the second antiferromagnetic phase observed below 2.15 K.

Encouraged by the consistency of the results indicating a dominant role of the Γ_5 ground state as a precursor to the magnetic phase transition, an estimate was made of the effective exchange and dipole fields using a molecular-field approximation. Using the calculated $g_\parallel$ factor of the Γ_5 ground states and the exchange energy based on the estimated intrinsic width of 3 cm^{-1} from the neutron data at 4.2 K (Fig. 1), we estimate an exchange field, H_{ex}, of 3.2 kG. Adopting the simple relations proposed by Bleaney[35] [i.e., $\lambda\chi^0=1$ and $H_{int}=\lambda M_0$, where χ^0 (6.786 emu/mole) is the calculated susceptibility at T_N(2.28 K) due to crystal-field effects alone, M_0 ($6.36\mu_B$ per Tb ion) is the saturated magnetization of the Γ_5 state, and λ is the molecular-field parameter], we find an effective internal field of $H_{int}=5.23$ kG. This is to be compared with the internal field of 4.5±0.15 kG estimat-

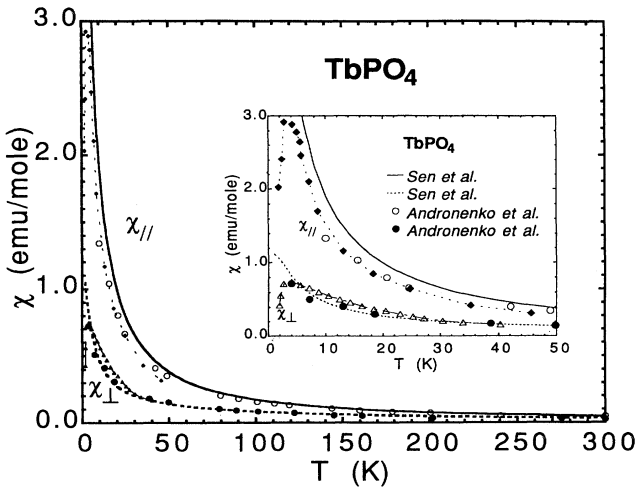

FIG. 5. The calculated (lines) and measured (symbols) magnetic susceptibility of $TbPO_4$ with the field directions perpendicular ($\chi_\perp$) and parallel ($\chi_\parallel$) to the crystallographic c axis. Inset: details of the temperature dependence of the susceptibility in the 9–50 K region.

ed from Zeeman-effect measurements by Böhm and co-workers.[5] Additionally, if we assume that $H_{int}=H_{ex}+H_{dip}$, then an effective field for the dipole interactions of $H_{dip}=2.08$ kG can be deduced. These effective-field strengths are, in general, of the same order-of-magnitude as those found for $HoPO_4$ and $ErPO_4$.[22,23]

The calculated crystal-filed contribution to the specific heat[22,36] C_{CF} is shown in Fig. 6 together with the measured specific-heat data obtained by Hill, Cosier, and Smith.[9] Since cooperative effects such as long-range magnetic ordering and structural transformation have not been incorporated in the crystal-field model, the calculated specific heat can only be compared with experimental data in the paramagnetic region. As can be seen from the inset of Fig. 6, the agreement between the experimental data and calculation is fairly good in the temperature range of 4–10 K. The Schottky-like peaks present near 3.8 and 45 K are the result of low-lying crystal-field states. In order to compare the calculated values with the measured total specific heat over a wide range of temperatures, contributions from other components such as lattice vibrations should be included. We are not aware, however, of any published specific data in the literature that extend to temperatures above 14 K.

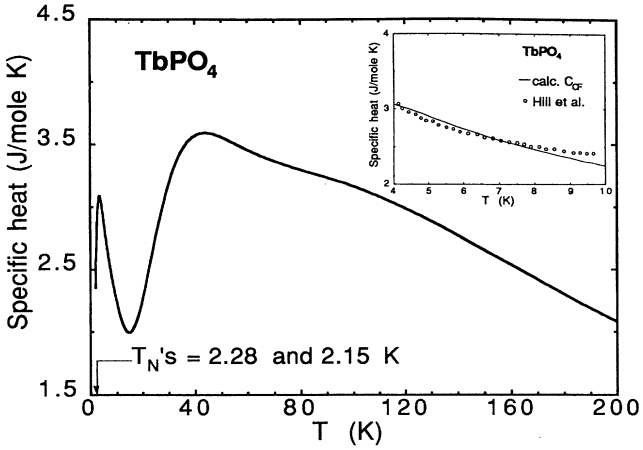

FIG. 6. The calculated contribution to the specific heat of $TbPO_4$ from the Tb ion-crystal-field states. Inset: comparison of the calculated and measured specific heat (Ref. 9) in the 4–10-K region.

IV. CONCLUSION

The crystal-field excitations within the $^7F_6$ ground multiplet of the Tb^{3+} ions in $TbPO_4$ have been measured by neutron scattering, and a set of crystal-field parameters has been determined by fitting the neutron data using a Hamiltonian that includes atomic free-ion and crystal-field interactions. The calculated excitation spectra satisfactorily account for all of the observed features in the neutron data at temperatures from 4.2 to 150 K, and the calculated energies of the high-lying $^5D_4$ multiplet agree with the optical data obtained previously by Böhm and co-workers.[5] We find that the crystal-field-level structure derived from the present analysis can provide a basis for explaining the magnetic properties of $TbPO_4$ at low temperatures. The calculated magnetic susceptibility agree well with the experimental data. The spectroscopic splitting g factors of the ground-state doublet, the saturated moments at low temperatures, and the estimated effective internal field are in good agreement with the values obtained by other workers from specific-heat, Zeeman-effect, and magnetization measurements. Hopefully, the present characterization of the ground-state wave functions for paramagnetic Tb ions in $TbPO_4$ will be useful for future extended studies of the magnetoelastic interactions and phase transitions in rare-earth orthophosphates.

ACKNOWLEDGMENTS

We thank J. Simon Xue and J. P. Hammonds for their assistance in characterization of the samples and in the neutron-scattering experiments. Work performed at Argonne and Oak Ridge National Laboratories is supported by the U.S. DOE, Office of Basic Energy Sciences, Chemical Sciences and Materials Sciences Divisions under Contract Nos. W-31-109-ENG-38 (ANL) and DE-AC05-84OR21400 (ORNL), respectively.

[1]J. Coing-Bayat, F. Sayetat, and A. Apostolov, J. Phys. (Paris) **36**, 1165 (1975).
[2]W. Nägele, D. Hohlwein, and G. Domann, Z. Phys. B **39**, 305 (1980).
[3]S. Spooner, J. N. Lee, and H. W. Moos, Solid State Commun. **9**, 1143 (1971).
[4]V. I. Sokolov, Z. A. Kazei, and N. P. Kolmakova, Physica B **176**, 101 (1992); also V. I. Sokolov, Z. A. Kazei, N. P. Kolmakova, and T. V. Solov'yanova, Zh. Eksp. Teor. Fiz. **99**, 945 (1991) [Sov. Phys. JETP **72**, 524 (1991)].
[5]W. Böhm, H. G. Kahle, and W. Wüchner, Phys. Status Solidi B **126**, 381 (1984); also W. Böhm, R. Herb, H. G. Kahle, A. Kasten, J. Laugsch, and W. Wüchner, *ibid.* **54**, 527 (1972).
[6]J. N. Lee, H. W. Moos, and B. W. Mangum, Solid State Commun. **9**, 1139 (1971).
[7]J. F. L. Lewis and G. A. Prinz, Phys. Rev. B **10**, 2892 (1974).
[8]G. A. Prinz and J. F. L. Lewis, J. Magn. Magn. Mater. **39**, 285 (1983).
[9]R. W. Hill, J. Cosier, and S. H. Smith, Solid State Commun. **26**, 17 (1978).
[10]M. Schwab and H. G. Kahle, Phys. Status Solidi B **84**, 167 (1977).
[11]H. Suzuki and T. Nakajima, J. Phys. Soc. Jpn. **47**, 1441 (1979).
[12]H. C. Schopper, Int. J. Magn. **3**, 23 (1972).
[13]H.-C. Schopper, P.-J. Becker, E. Böhm, G. Dummer, H. G. Kahle, L. Klein, and G. Müller-Vogt, Phys. Status Solidi B **46**, K115 (1971).
[14]S. I. Andronenko, A. N. Bazhan, L. P. Mezentseva, I. A. Bondar', and V. A. Ioffe, Fiz. Tverd. Tela (Leningrad) **26**, 2473 (1984) [Sov. Phys. Solid State **26**, 1497 (1985)].
[15]G. T. Rado, J. M. Ferrari, and W. G. Maisch, Phys. Rev. B **29**, 4041 (1984).

[16]H. Sen, D. Heogy, and B. M. Wanklyn, J. Magn. Magn. Mater. **73**, 221 (1988).
[17]J. Sivardiere, Phys. Rev. B **8**, 2004 (1973).
[18]H. Saji, T. Yamadaya, and M. Asanuma, J. Phys. Soc. Jpn. **28**, 913 (1970).
[19]S. Bluck and H. G. Kahle, J. Phys. C **21**, 5193 (1988).
[20]H. Mensinger, J. Jakelski, H. G. Kahle, A. Kasten, and W. Paul, J. Phys.: Condens. Matter **5**, 935 (1993); C. Anderer, G. Hess, and H. G. Kahle, *ibid.* **5**, 945 (1993); and A. U. Müller, J. Jakelski, and H. G. Kahle, *ibid.* **5**, 955 (1993).
[21]G. Üffinger and A. Kasten, Phys. Status Solidi B **128**, 201 (1985); A. Kasten and G. Üffinger, *ibid.* **128**, 525 (1985).
[22]C.-K. Loong, L. Soderholm, M. M. Abraham, L. A. Boatner, and N. M. Edelstein, J. Chem. Phys. **98**, 4214 (1993).
[23]C.-K. Loong, L. Soderholm, J. P. Hammonds, M. M. Abraham, L. A. Boatner, and N. M. Edelstein, J. Appl. Phys. **73**, 6069 (1993); C.-K. Loong, L. Soderholm, J. P. Hammonds, M. M. Abraham, L. A. Boatner, and N. M. Edelstein, J. Phys.: Condens. Matter (to be published).
[24]M. M. Abraham, L. A. Boatner, T. C. Quinby, D. K. Thomas, and M. Rappaz, Radioactive Waste Management **1**, 181 (1980).
[25]W. O. Milligan, D. F. Mullica, G. W. Beall, and L. A. Boatner, Inorg. Chim. Acta **60**, 39 (1983).
[26]C.-K. Loong, S. Ikeda, and J. M. Carpenter, Nucl. Instrum. Methods A **260**, 381 (1987); C.-K. Loong, J. M. Carpenter, and S. Ikeda (unpublished).
[27]L. A. Boatner and B. C. Sales, in *Radioactive Waste Forms for the Future,* edited by W. Lutze and R. C. Ewing (Elsevier Science, Amsterdam, 1988), Chap. 8.
[28]Von H. Schwarz, Z. Anorg. Allg. Chem. **323**, 44 (1963).
[29]W. Marshall and S. W. Lovesey, *Theory of Thermal Neutron Scattering* (Oxford University Press, Oxford, 1971).
[30]B. G. Wybourne, *Spectroscopic Properties of Rare Earths* (Wiley, New York, 1965).
[31]H. M. Crosswhite and H. Crosswhite, J. Opt. Soc. Am. B **1**, 246 (1984).
[32]W. T. Carnall, G. L. Goodman, K. Rajnak, and R. S. Rana, J. Chem. Phys. **90**, 3443 (1989).
[33]J. H. van Vleck, *The Theory of Electric and Magnetic Susceptibilities* (Oxford University Press, London, 1932).
[34]E. Pytte and K. W. H. Stevens, Phys. Rev. Lett. **27**, 862 (1971).
[35]B. Bleaney, Proc. R. Soc. London Ser. A **276**, 19 (1963).
[36]R. Saez Puche, M. Norton, T. N. White, and W. S. Glaunsinger, J. Solid State Chem. **50**, 281 (1983).